Received: 22 November 2022 | Revised: 12 January 2023 | Accepted: 13 January 2023

DOI: 10.1002/jbio.202200361

RESEARCH ARTICLE

JOURNAL OF BIOPHOTONICS

Comparative study of in-vitro autofluorescence of normal versus non-melanoma-skin-cancer cells at different excitation wavelengths

Federico Garbarino[1,2] | **Daniel Scelfo**[3] | **Gabriele Paulone**[3] | **Alessia Paganelli**[1,2] | **Alessandro Ulrici**[4] | **Cristina Magnoni**[1] | **Luca Pasquali**[3,5,6]

[1]Department of Dermatology, Surgical, Medical and Dental Department of Morphological Sciences Related to Transplant, Oncology and Regenerative Medicine, University of Modena and Reggio Emilia, Modena, Italy

[2]Clinical and Experimental Medicine, University of Modena and Reggio Emilia, Modena, Italy

[3]Department of Engineering "Enzo Ferrari", University of Modena and Reggio Emilia, Modena, Italy

[4]Department of Life Sciences, University of Modena and Reggio Emilia, Reggio Emilia, Italy

[5]IOM-CNR, Trieste, Italy

[6]Department of Physics, University of Johannesburg, Auckland Park, South Africa

Correspondence
Luca Pasquali, Department of Engineering "Enzo Ferrari", Universty of Modena and Reggio Emilia, Via Vivarelli 10, 41125 Modena, Italy.
Email: luca.pasquali@unimore.it

Funding information
Fondazione Cassa di Risparmio di Modena, Grant/Award Number: FAR2019 - INTER - line FCRM - project "LUMINA

Abstract

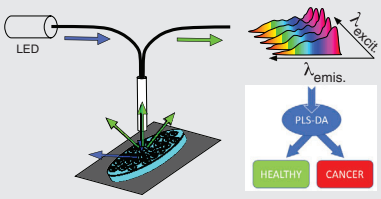

In this experimental study the autofluorescence of squamous carcinoma cells, stimulated by 6 different excitation wavelengths in the range 280–533 nm, has been compared with the autofluorescence of normal control keratinocytes. Skin cells were cultivated in vitro, to isolate their characteristic autofluorescence form the more complex one that would be originated by the complete skin tissue. Autofluorescence spectra in the visible range were complemented by absorption measurements. It was observed that the control cells showed characteristic emission (and absorption) structures due to typical endogenous chromophores [FAD and NAD(P)H, lipo-pigments, porphyrins], that were severely dumped in pathological cells. The autofluorescence spectra were then elaborated by multivariate analysis: after a first exploratory data analysis by means of Principal Component Analysis, the whole dataset was used to develop classification models using partial least squares-discriminant analysis, to differentiate between normal and pathological cells. This permitted us to identify the most suitable fluorescence spectral interval, in the 550–670 nm range, to discriminate between normal and pathological behavior, independently on the excitation wavelength.

KEYWORDS
autofluorescence, keratinocytes, multivariate analysis, non-melanoma skin cancer, squamous-cell carcinoma

Abbreviations: AF, autofluorescence; LV, latent variables; NMSC, non-melanoma skin cancer; PBS, phosphate buffered saline; PCA, principal component analysis; PLS-DA, partial least squares-discriminant analysis; SCC, squamous cell carcinoma; VIP, variable importance in projection.

1 | INTRODUCTION

Optical luminescence for diagnostic purposes in medicine is a well-developed field [1, 2]. Techniques based on the

detection of luminescence are fast, noninvasive, and quantitative. Fluorescence at certain wavelengths can be typically induced in tissues by treating them with fluorescent markers that bind to selected receptors. Besides this, the study of intrinsic fluorescence [autofluorescence (AF)] of different bio-molecules is becoming more and more important. AF of specific cells, matrices and bio-molecules is strictly related to their morpho-functional properties. Alterations of these properties, for example, due to pathologies like tumors, can induce strong modification of AF [3–9]. Most important endogenous fluorophores are molecules largely present in living systems, like structural proteins, aromatic amino acids, enzymes, flavins, lipopigments, porphyrins, collagen and elastin fibers, to cite some [1–3, 10]. After excitation with monochromatic light at specific wavelength, these systems emit characteristic luminescence at higher wavelengths. The spectral lineshape and intensity of the different spectral regions depend on the bio-molecules and their concentration. On the other hand, in most cases the recorded signals are complicated: not only because the lineshapes of the specific fluorophores are broad and are partially superimposed, but also because multiple fluorophores are typically present, adding up their contributions.

Due to its clear potential, the field is in rapid expansion. Most studies are carried out directly in vivo, where the signal is complicated further, due to the contribution of different emitters: fluorophores inside cells, in the connective tissue and from the blood/fluids. Moreover, a great variability can be found in different individuals or in different sampled regions of the same individual. Moreover, a pathological alteration can affect the contributions from the constituents in a different way, making the analysis intricate.

In the present study we focus our attention on AF produced by isolated skin cells grown in vitro, comparing the signal of non-cancerous versus neoplastic keratinocytes [squamous cell carcinoma (SCC)]. Non-melanoma skin cancer (NMSC) is the most common type of skin cancer in Caucasian people, with an increasing of incidence worldwide [11]. A critical factor for dermatologists is the early diagnosis, to provide proper treatment. Surgical excision with clear margins represents the best approach to reduce the rate of recurrence. AF spectroscopy would provide a powerful and fast diagnostic tool to guide the correct early treatment of the affected areas of the skin [12]. It was recently demonstrated by some of us that AF spectroscopy can be used as an optical biopsy tool, for the early detection of NMSC ex vivo [13]. It was found that the overall intensity of the fluorescence emission in NMSC tissues reduced sizably compared to tissues in healthy conditions. The present study extends this investigation, focusing on the sole contribution of keratinocytes. This type of study, where single contributors to luminescence are considered, is still quite rare in the literature.

AF was measured both on cell pellets and normal saline cell suspension (PBS) at different wavelengths of the excitation light. In particular, commercially available light emitting diodes (LEDs) were adopted as excitation sources, working at λ_{exc} = 280, 310, 365, 405, 470, and 533 nm.

Multivariate analysis of the emitted fluorescence spectra was then performed to get quantitative information, to provide a method that clearly disentangles normal and pathological situations and to emphasize those spectral regions that appear more meaningful as far as the classification between normal and cancerous cells is concerned. Multivariate analysis-based approaches for the differentiation between AF spectra measured on healthy and cancer cells have already been successfully applied in the literature [14–16]. In the present study, multivariate analysis of the AF spectra was performed in two subsequent steps. The first step consisted in an unsupervised exploratory analysis performed by calculating principal component analysis (PCA) models separately for each group of AF spectra measured at a given excitation wavelength. Then, in the second step, all the AF spectra measured at the six excitation wavelengths were merged in a unique dataset and subjected to multivariate classification by means of partial least squares-discriminant analysis (PLS-DA). Different spectra preprocessing methods were tested, and the corresponding classification models were validated by means of an external test set. The performance of the best performing classification model was also further verified by means of a permutation test.

Our group already demonstrated the ex-vivo hypofluorescent aspect of cutaneous neoplasms [13]. However, several well-known dermal and epidermal chromophores could give reason of such findings (e.g., hemoglobin, collagen, keratins of the stratum corneum); therefore, whether cancerous cells specifically could be (or, at least, partially) responsible for NMSC hypofluorescence remained to be clarified [5, 17]. The goal of the present study is to assess AF changes in SCC cells compared to healthy keratincoytes, in the absence of possible adjacent tissue interferences.

2 | EXPERIMENTAL SECTION

2.1 | Cell cultures

UPCI:SCC154 cell line was used for in vitro evaluation of the behavior of tumoral cells from cutaneous squamous cell carcinoma (SCC).

Control keratinocytes (primary cells) were obtained from cutaneous discarded material from different donors undergoing elective surgery at Dermatologic Surgery Unit, Modena University Hospital. In particular, 3-donor pool keratinocytes were initially co-seeded with mitomycin-treated 3 T3 murine fibroblasts to promote epithelial cell growth.

Cells were plated into 75 cm^2 culture flasks at a density of 10^6 cells/flask. Trypan blue was used for the assessment of cell viability. To increase the luminescence signal form cells and avoid signal contamination due to the culture solution, AF was measured on cell pellets. The pellets were then put on a suitable support (see below) and care was taken in acquiring AF immediately after removing the cells from the solution, in order to minimize deterioration.

2.2 | Optical setup

Fluorescence spectra were recorded with an Ocean Insight QEPRO-FL high sensitivity spectrometer working in the wavelength range between 348 and 1132 nm. High power LEDs from Ocean Insight (model LSM LEDs) were used as excitation sources, with emission wavelengths centered at 280, 310, 365, 405, 470, and 533 nm, FWHM <20 nm (36 nm for $\lambda_{exc} = 533$ nm). Solarization-resistant UV–visible optical fibers were used to transport light to the cell samples and to collect the luminescence signal and send it to the spectrometer. A sketch of the experimental apparatus is shown in Figure 1A,B. In Figure 1A the configuration used to measure luminescence from the cell pellets is reported. A solarization-resistant coaxial reflection/backscattered probe was used. Cell pellets were deposited on a Petri plastic transparent dish with a black light-absorbing paper placed on the back, to reduce luminescence contributions from scattered light on the dish support. The support was custom designed to allow for a variable tilt angle between the impinging/collection direction and the Petri plate, to avoid a direct reflection of the incident excitation light in the collection channel and reduce possible AF phenomena from the optical fiber itself. A system to control precisely the probe height with respect to the sample was also implemented, to reproduce strictly the sampling geometries for the different replicas of the cell samples. Care was taken to disentangle the luminescence signal of the cells from the possible contribution of the support. Different supports were therefore tested (plastic Petri dishes, Eppendorf test tubes, multiwells), at different incidence and detection angles. Petri transparent dishes, with the black light-absorbing paper positioned at the back and at a tilt angle of 30° were seen to provide the best results in terms of negligible incident light backscattering and negligible luminescence from the sample holding system. An interferential, high pass, linear variable filter (Ocean Insight, model LVF-H) was also used to cut the excitation wavelength in the measurement channel and to avoid saturation of the spectrometer.

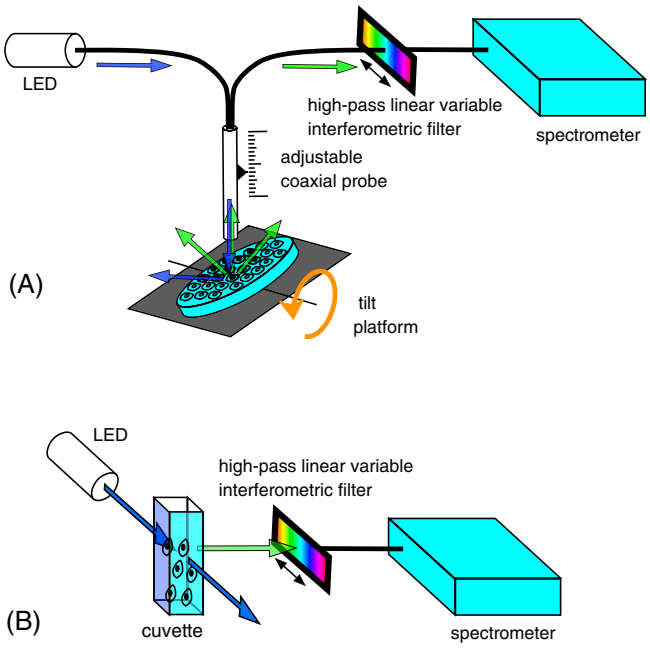

FIGURE 1 (A) Scheme of the experimental apparatus used to measure fluorescence from cells deposited on a Petri dish. (B) Scheme of the apparatus used to measure fluorescence from cells in liquid suspension.

Figure 1B illustrates the configuration adopted to measure the luminescence of suspended cells in normal saline solution (0.9%). In this case, quartz optical cuvettes were used and light was collected at perpendicular direction with respect to the impinging beam.

Transmission spectra were also recorded to flank the luminescence results, using a balanced deuterium and tungsten halogen source (DH-2000-BAL Light Source from Ocean Insight) and a miniature spectrometer (USB4000-XR1 from Ocean Insight). Cells supported on a transparent Petri dish were used for transmission experiments.

2.3 | Multivariate analysis

The set of AF spectra measured over a period of 7 months on cells deposited on Petri dishes, which were considered due to the higher signal-to-noise ratio with respect to the spectra measured in solution, was subjected to multivariate analysis.

Each spectrum contains the intensity values measured at 1044 wavelengths in the range between 348 and

1132 nm. The dataset includes all the spectra acquired using the six different excitation wavelengths; in particular, eight spectra (four on healthy samples and four on NMSC samples) measured for each one of the 280, 310, and 365 nm excitation wavelengths, and seven spectra (four on healthy samples and three on NMSC samples) measured for each one of the 405, 470, and 533 nm excitation wavelengths.

2.3.1 | Separate PCA models for each excitation wavelength

As a first step, each group of spectra measured at a given excitation wavelength was explored separately from the others by means of PCA, which is an unsupervised technique used to reduce the data dimensionality while preserving the original structure of the dataset. In the present work, PCA was used to evaluate whether, for each excitation wavelength, the pattern of the corresponding emission spectra of healthy samples was somehow different from the pattern of the spectra measured on NMSC samples, thus without forcing any separation between the two classes.

To this aim, for each group of spectra measured at a given excitation wavelength, two PCA models were calculated, corresponding to two variable preprocessing methods: mean centering and autoscaling. Mean centering consists in transforming each variable by subtracting its mean value from all the observations, while autoscaling consists in mean centering and then dividing by the variable standard deviation.

In addition to assessing whether differences were observable between healthy and NMSC samples, PCA also allowed to investigate which excitation wavelengths led to the best separation between the two classes, and to identify the most relevant spectral regions.

2.3.2 | PLS-DA classification models on the whole dataset

The second step of multivariate analysis consisted in calculating classification models on the whole dataset of spectra, in order to evaluate the possible presence of common spectral regions for all the excitation wavelengths where the AF spectra present different patterns for healthy and NMSC cells. The whole dataset, including 24 spectra measured on healthy cells and 21 spectra measured on NMSC (SSC) cells, was analyzed by means of PLS-DA. To this aim, the dataset was first randomly divided in a training set including 30 spectra and in a test set including the remaining 15 spectra, taking care to include spectra for each excitation wavelength and each class in both the training and the test set, as reported in Table S1 (provided as supporting information).

The training set was then used to calculate two PLS-DA models, one considering mean centering and one considering autoscaling as preprocessing method. The optimal dimensionality of each PLS-DA model, that is, the number of Latent Variables (LVs) leading to the minimum classification error, was selected by random cross validation, which was performed subdividing the training set samples in five deletion groups and repeating the crossvalidation for 20 iterations. Both the models were then validated by means of the test set samples. The classification performance of the PLS-DA models was evaluated considering their classification efficiency (EFF), calculated as the geometric mean of sensitivity (SENS) and specificity (SPEC). SENS is the percentage of samples of the modelled class correctly accepted by the class model, SPEC is the percentage of objects of the other classes correctly rejected by the class model, and EFF is the geometric mean of SENS and SPEC. Since for a two-class PLS-DA model like in the present case (healthy and NMSC classes) the SENS value of class 1 is equal to the SPEC value of class 2, and the SPEC value of class 1 is equal to the SENS value of class 2, the EFF value for both the classes is the same. The EFF, SENS, and SPEC parameters were computed considering the values calculated on the training set (EFF_{CAL}, $SENS_{CAL}$, $SPEC_{CAL}$), those estimated in crossvalidation (EFF_{CV}, $SENS_{CV}$, $SPEC_{CV}$), and the values predicted for the test set (EFF_{PRED}, $SENS_{PRED}$, $SPEC_{PRED}$).

Considering the relatively limited number of AF spectra available to perform multivariate classification, to further verify the statistical significance of the PLS-DA model showing the best overall performance, a permutation test was also implemented. The permutation test essentially consisted in repeatedly and randomly reassigning the samples to the two classes, both for the training and for the test set. For each one of the 100 permutations considered in the present work, a PLS-DA model was calculated on the training set considering the same number of LVs of the correct model and the same crossvalidation procedure, and then it was applied to the test set. For each permutation, the values of EFF_{CAL}, EFF_{CV}, and EFF_{PRED} were calculated. Finally, the distributions of the EFF_{CAL}, EFF_{CV}, and EFF_{PRED} values of the 100 permutations were compared with the corresponding values of the correct model, using a one-tailed t test to verify whether its EFF values were statistically significant ($p = 0.05$).

The PCA and PLS-DA models were calculated using the functions available in the PLS-Toolbox ver. 8.9.2 (Eigenvector Research Inc., Manson, WA, USA) running in the Matlab ver. 9.10 (R2021a) environment (The MathWorks Inc., Natick, MA, USA). The permutation test was calculated using a Matlab function written ad hoc.

3 | RESULTS AND DISCUSSION

3.1 | AF spectra

AF spectra were recorded for different batches of the normal and SSC cells. In spite that extreme care was taken in reproduce accurately the same experimental conditions, an intrinsic variability of the signals was observed when measuring different batches from the same cells. While the major spectral characteristics were preserved comparing samples with equivalent number of cells, the spectral intensities could vary from sample to sample. To

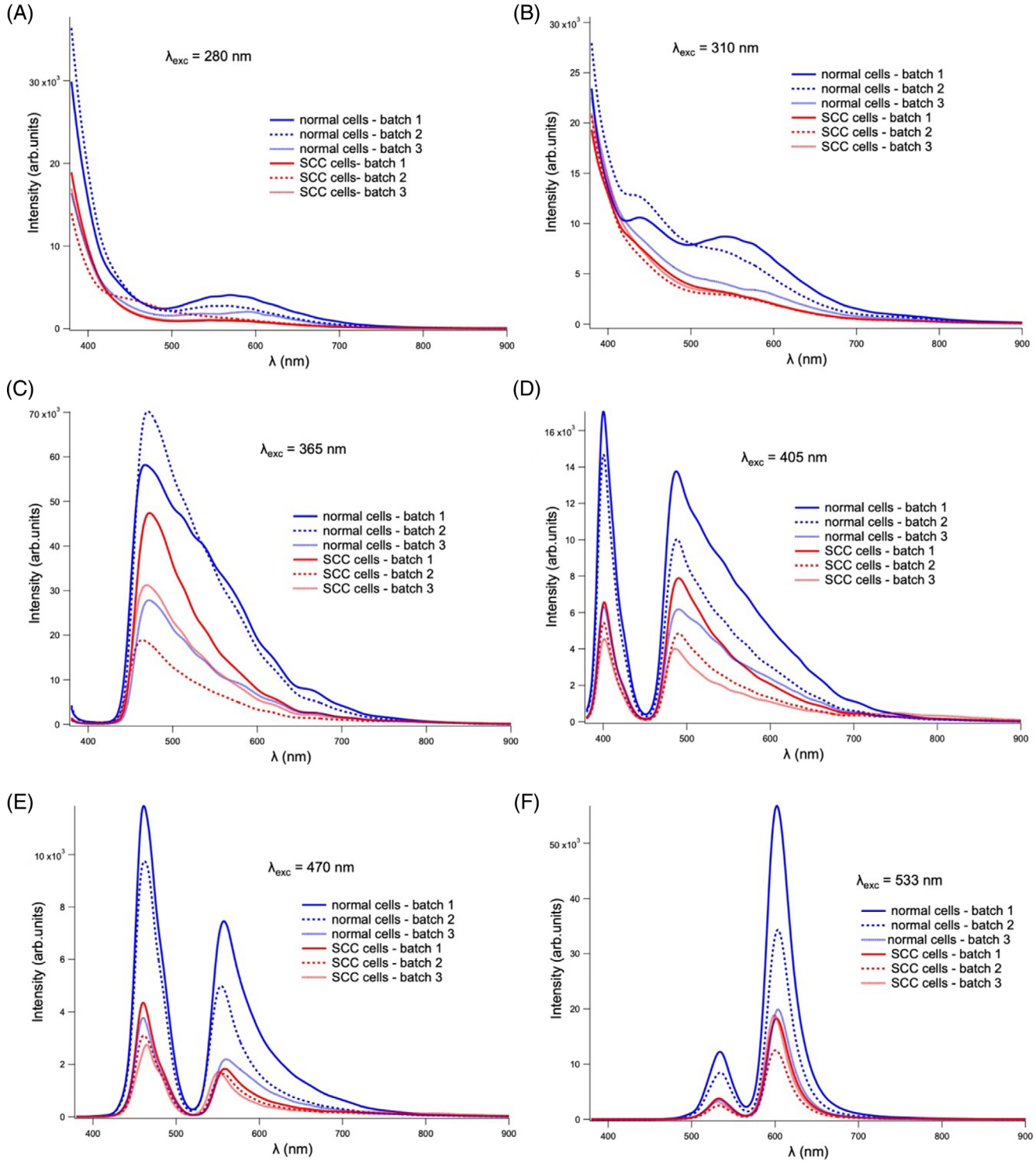

FIGURE 2 AF spectra taken at different excitation wavelengths on three batches (each batch is measured in the same day and under identical experimental conditions) of normal and SCC cultivated cells. All batches refer to 5 million cultivated cells.

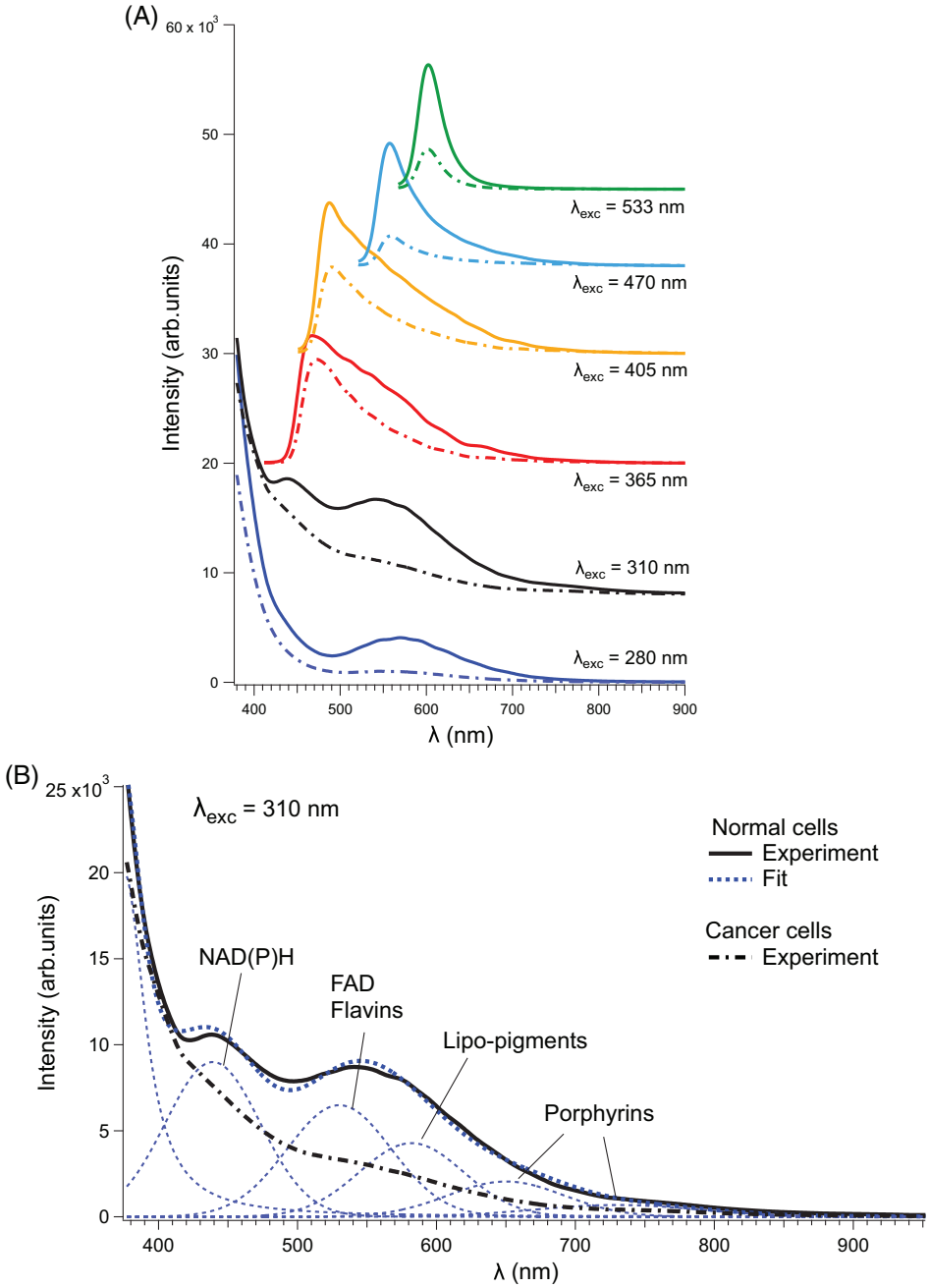

FIGURE 3 (A) AF spectra as obtained at increasing excitation wavelengths. Continuous lines refer to normal cells and broken lines to NMSC (SCC) cells. (B) The fluorescence spectrum taken with $\lambda_{exc} = 310$ nm is shown, together with a best-fit decomposition of features using Gaussian profiles.

give an idea, in Figure 2 we compare the AF spectra of three virtually identical batches of normal and SCC cells samples excited at the different wavelengths. Although the intensity variations can be quite considerable from batch to batch, comparing the normal and SCC signals within the same batch at a given excitation wavelength, it can be observed that SCC cells are in general less emitting than normal cells, at all emission wavelengths. Interestingly, above 400 nm of excitation wavelength, the adopted linear interferential filter is not capable to cut completely the frequency of the excitation radiation and some degree of backscattering is observed as peaks appearing at 405, 470, and 533 nm in Figure 2D–F, respectively. Although the analysis of the backscattered radiation is not the objective of the present work, it can be seen that the backscattering signal within the same batch in general also reduces for SCC cells compared to normal ones.

In spite of the intrinsic variability, an overall distinctive behavior of normal and neoplastic cells is observed. In Figure 3A the most representative spectra are reported, referred to 5 million cultivated cells, both for normal and SSC keratinocytes (batch 1 of Figure 2). In this case, the backscattering contribution in the spectra taken at $\lambda_{exc} > 400$ nm has been removed, to highlight only AF emission. Normal cells show well defined

features which appear more distinct when excited in the UV spectral range (λ_{exc} = 280, 310, and 365 nm). The lineshape results progressively less structured as long as the excitation energy decreases (the wavelength increases). In all investigated cases and for all excitation wavelengths the SCC cells present a drastic reduction of AF in all regions with respect to the normal cells. The spectral features are also less defined.

In Figure 3B the AF spectrum excited with photons at λ_{exc} = 310 nm, where spectral features appear more evident, has been decomposed with multiple Gaussian peaks in a least-squares fitting. Major contributions in normal cells can be associated to characteristic luminescence from coenzymes nicotinamide adenine dinucleotide (phosphate) NAD(P)H, centered at about 440 nm, and flavin-adenin dinucleotide (FAD), at about 530 nm, which can be influenced by metabolic alterations [1, 2, 12, 18]; higher wavelength structures can be associated to lipo-pigments, with maximum at 580 nm, and to porphyrins, at 650 nm and above 700 nm [19]. It is important to notice that all contributions are strongly depressed in the cancerous cells. This is in general agreement with observations also made in vivo [6, 13, 20, 21]. FAD and NAD(P)H are metabolic coenzymes involved in the electron transport chain which are very sensitive to neoplastic alterations [22]. Their luminescence reduction in cancer cells is compatible with a change in the coenzymes redox state. While NAD(P)H is luminescent in the reduced state, flavins are luminescent in the oxidized state. The conversion of FAD to its reduced form has been previously reported during cancer progression in vivo [18], which results in luminescence reduction. On the other hand, NAD(P)H oxidation typically occurs in neoplastic cells with increased metabolism, due to its involvement in ATP and energy production [1, 22]. This also contributes to the reduction of the luminescence. Regarding the signal of porphyrins, the decrease observed in this work seems to contrast the observations made in vivo, where an increase was sometimes measured [19]. This effect could be related to the more complex scenario that is present in skin tissues in vivo, where more components contribute to the luminescence. The role of blood drainage in skin tissues for example could play a fundamental role in this respect [19]. The decomposition of the spectra acquired at the other excitation wavelengths, or for SCC cells, is not shown here, since these spectra appear generally less structured compared to those of the normal cells excited with UV light. This may be related to the fact that UV radiation is more efficient in the excitation of the luminescent chromophores [1, 2, 8, 12]. Although, we are not interested here in the relative intensities of the different components recorded at the different excitation wavelengths. Instead, the decomposition of

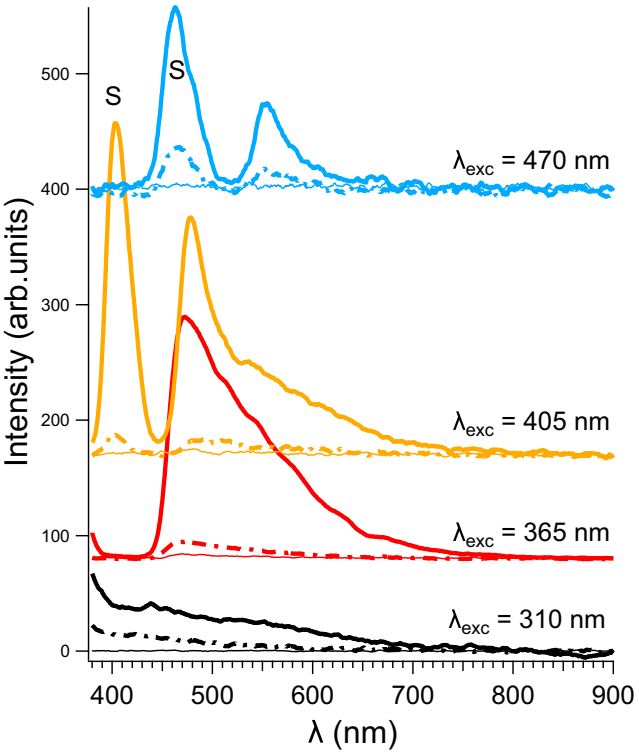

FIGURE 4 Luminescence spectra acquired on cells suspended in saline solution. Continuous lines refer to normal cells and broken lines to SSC cells. The signal backgrounds, obtained with no cells in the physiological solution, are also reported as a thin continuous line. Labels "S" refers to scattered radiation of the excitation beam.

Figure 3B is mostly informative on the main chromophore species contributing to the signals in the different spectral regions and, indeed, all spectra taken at higher wavelength than 310 nm present broad emission in intervals covered by these chromophores.

The spectra shown in Figures 2 and 3 were obtained by separating the cells from the saline solution, so to increase the density of emitters in the probed area of the impinging beam and therefore increase the luminescence. To validate the results, further luminescence spectra were also taken with the cells still in saline solution, exploiting the experimental setup shown in Figure 1B.

AF spectra acquired from the cells in saline solution are reported in Figure 4. Although the overall luminescence signal is much lower with respect to the spectra of Figures 2 and 3 at all the probed excitation wavelengths, the same general trend is confirmed. At all excitation energies, the luminescence of the normal cells is always stronger than the pathological ones. Some excitation photons (i.e., at λ_{exc} = 365 and 405 nm) seem to induce a stronger luminescence intensity in the normal cells in the AF spectral region around 500 nm with respect to the other used photons, but this would need further

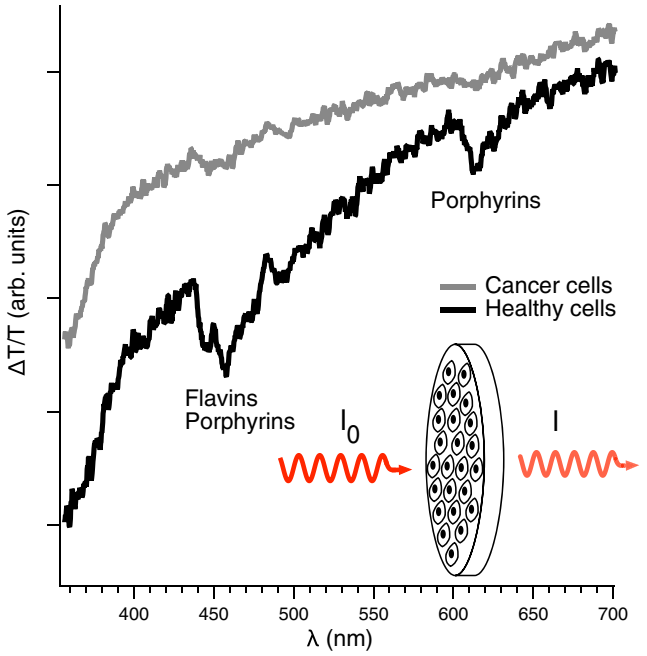

FIGURE 5 ΔT/T spectra acquired on normal and cancer cells at comparable cell density. $\Delta T/T = (T_{Petri + cells} - T_{Petri})/T_{Petri}$. A scheme of the transmission experiment is shown in the inset. T refers to the measure of the ratio between the beam intensity I after passing the sample and the I_0 intensity (with no sample), as a function of the wavelength.

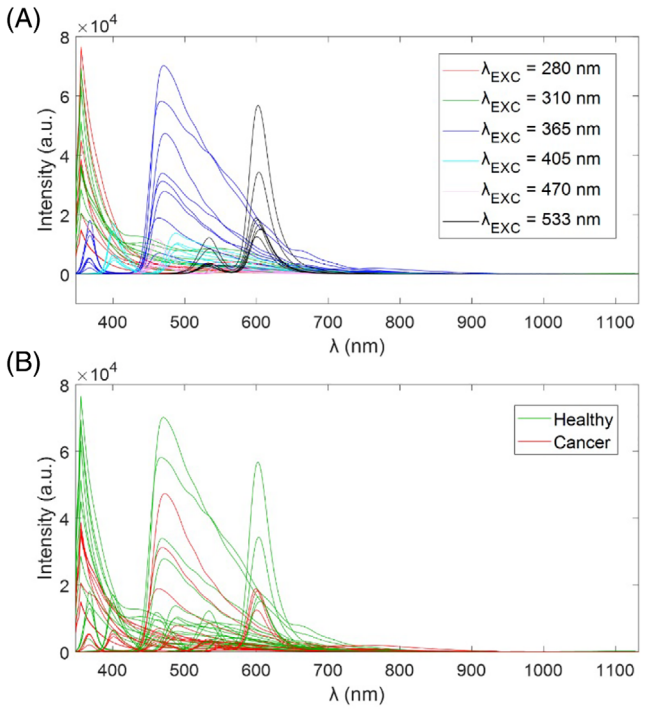

FIGURE 6 Dataset of AF spectra subjected to multivariate analysis, colored according to the different excitation wavelength (A) and according to the class of samples (B).

confirmation and it is not the subject of the present study. Although attenuated by the linear interferential filter, some amount of scattered light, labeled "S" in Figure 4, is observed for λ_{exc} above 400 nm. It can be noticed that again the scattered light from normal cell is much higher than the pathological counterparts. The reason for the augmented scattering in normal cells may be complex to explain, being related to the size as well to the refractive index of the cells and their constituting elements [23]. This is outside the scope of the present work and would deserve a separate study. On the other hand, this clear behavior could be also be used to recognize normal versus pathological cells.

Last but not least, absorption experiments in transmission have been performed on a continuous and uniform layer of normal and SSC cells supported (grown) on a plastic Petri dish at comparable cell density. The results are shown in Figure 5.

To highlight the contribution of the absorption of the cells, the spectra are shown in ΔT/T mode, that is subtracting the transmission T_{Petri} of the clean Petri from the transmission $T_{Petri + cells}$ of the cells + Petri and dividing by the transmission of the clean Petri. Again, in Figure 5 the cells show a distinctive behavior: in particular the control cells present definite absorption features that can be related to flavins and porphyrins [2, 12] that are almost absent, or strongly depressed, in SSC cells. Moreover, the differential transmission of normal cells in the region 500–600 nm and below 400 nm shows an overall more pronounced slope, which can be related to a generalized higher absorption with respect to SCC cells. These findings support further the results of luminescence discussed above, claiming for a reduction of NAD(P)H, FAD and flavins/porphyrins contribution in the cancerous cells.

3.2 | Multivariate analysis of AF spectra

The above reported results seem to indicate a distinctive behavior of normal versus pathological cells that is relatively independent on the excitation wavelength. But since the AF spectra are indeed affected by some level of intrinsic variability, as noted above, we adopted an approach based on multivariate analysis to address the possibility to distinguish unambiguously solely from the luminescence signals normal cells from pathological cells. To this aim, the AF spectra acquired using the instrumental setup depicted in Figure 1A (cells deposited on Petri dishes) were considered, since it led to overall luminescence signals much higher than those recorded on cells suspension. The whole set of AF spectra is reported in Figure 6, colored both according to the different excitation wavelengths (Figure 6A), and according to

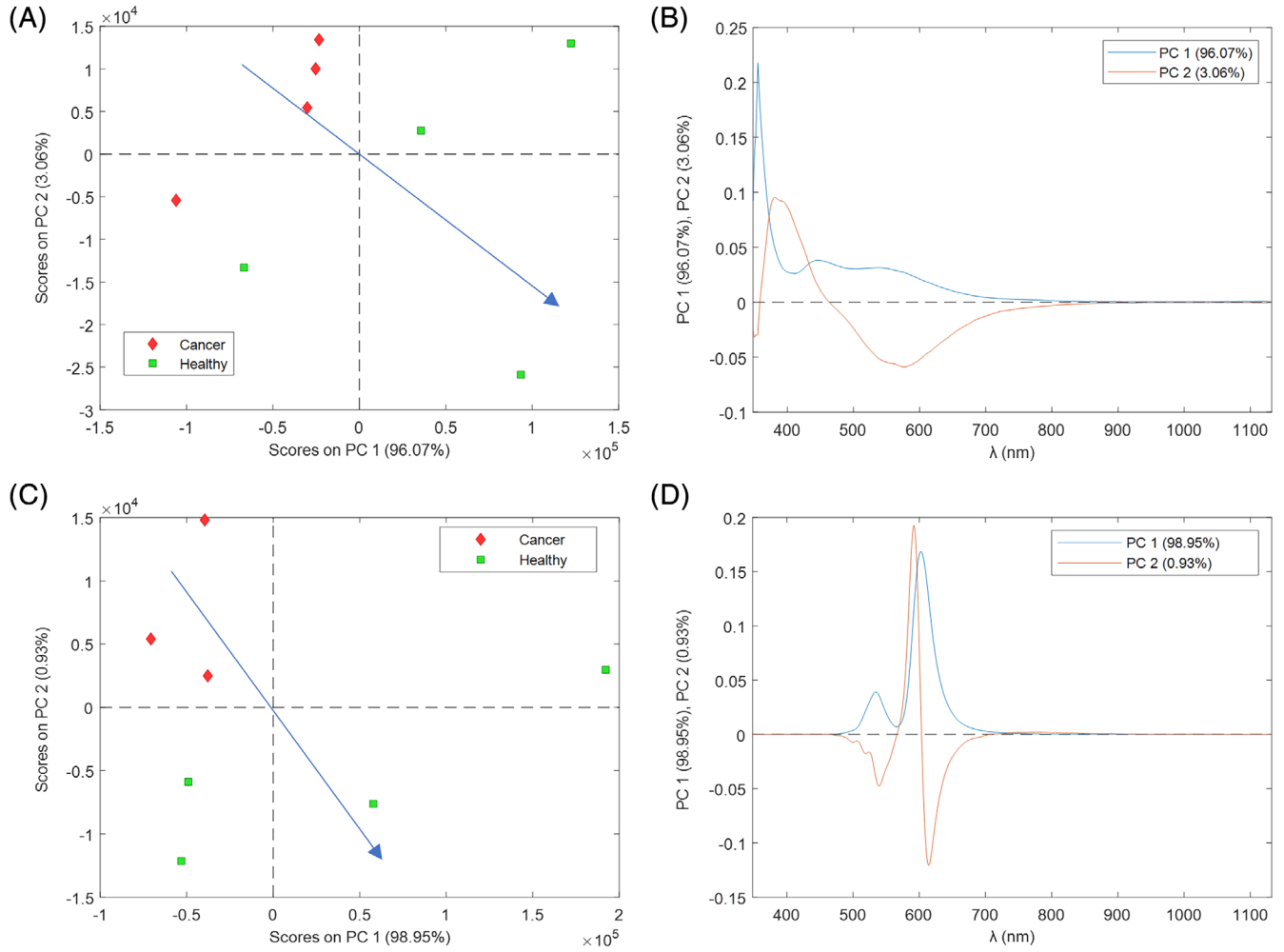

FIGURE 7 PC1-PC2 score plot (A) and loading plot (B) of the AF spectra measured at $\lambda_{exc} = 310$ nm, and PC1-PC2 score plot (C) and loading plot (D) of the AF spectra measured at $\lambda_{exc} = 533$ nm. The blue arrows in plots (A) and (C) represent the direction along which healthy and cancer (NMSC) cells can be separated from each other.

the class of samples (Figure 6B). As it was clearly expected, the spectral signatures differ mainly due to the different excitation wavelengths. It should be noted that the spectra presented in Figure 6 also include some contributions (peaks) due to the backscattered excitation wavelengths, whenever these fall in the spectral range measured by the spectrometer (348–1132 nm) and the interferential, high pass, linear variable filter is not able to completely suppress them. These peaks were in any case included in the multivariate analysis, since they also seem informative of the nature of the cells, as noted above.

3.2.1 | PCA of the AF spectra from single excitation wavelengths

Firstly, an exploratory data analysis was conducted by calculating separate PCA models on the groups of spectra measured at each excitation wavelength, in order to further verify that, based on an unsupervised approach, the patterns of spectra measured at a given excitation wavelength on healthy cells differ from those measured on cancer cells. As an example, Figure 7 reports the PC1-PC2 score and loading plots of the PCA models calculated on the mean centered spectra measured at $\lambda_{exc} = 310$ nm and at $\lambda_{exc} = 533$ nm.

Both the PC1-PC2 score plots (Figure 7A,C for $\lambda_{exc} = 310$ and 533 nm, respectively) show that the AF signals acquired on the NMSC cells are separate from the healthy cells; the two blue arrows have been added to highlight the directions along which the two groups can be separated from each other. Moreover, it can be observed that the AF signals of healthy cells are more spread with respect to those measured on NMSC cells, which indicates that the signals measured on healthy cells show a greater variability with respect to those measured on NMSC cells. The corresponding loading plots

TABLE 1 Results of the PLS-DA models calculated on the whole dataset of AF spectra considering the 550–850 nm range

Preprocessing method	LVs	$SENS_{CAL}$	$SPEC_{CAL}$	EFF_{CAL}	$SENS_{CV}$	$SPEC_{CV}$	EFF_{CV}	$SENS_{PRED}$	$SPEC_{PRED}$	EFF_{PRED}
Mean center	3	100.0%	68.8%	82.9%	93.2%	65.3%	78.0%	100.0%	87.5%	93.5%
Autoscale	4	100.0%	75.0%	86.6%	95.0%	66.9%	79.7%	100.0%	87.5%	93.5%

Note: The Sensitivity (SENS) and Specificity (SPEC) values are referred to the class of the cancer (NMSC) cells, while classification efficiency (EFF) is the geometric mean of SENS and SPEC.

reported in Figure 7B,D show the spectral regions that mainly contribute to the separation between the two groups. A similar behavior was observed, either in the PC1-PC2 or in the PC1-PC3 space, for all the excitation wavelengths (data not reported for conciseness reasons). In general, excluding the lower wavelength spectral regions, where contributions from some of the excitation wavelengths are present in some cases, the region common to all the AF spectra where the PCA loading vectors showed the highest absolute values was the one between 550 and 850 nm. This is a relevant region also for applications, since for measurements in vivo, this offers the opportunity to use, for excitation, photons in the visible range, which can be more practical. We stress, in any case, that the emission region above 550 nm appears to be the informative one for all datasets, including those obtained with excitation in the UV.

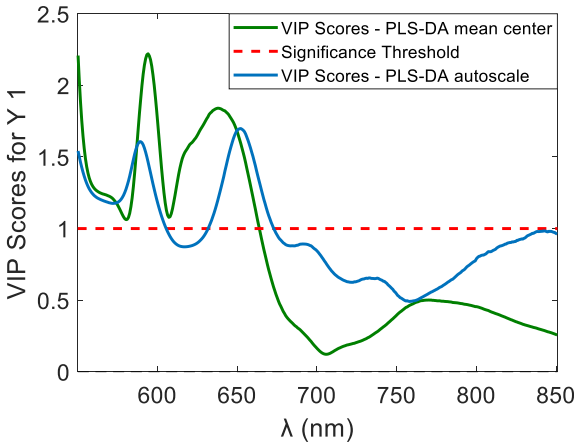

FIGURE 8 VIP scores of the PLS-DA models calculated on mean centered variables (green line) and on autoscaled variables (blue line)

3.2.2 | PLS-DA classification of the AF spectra

Since for each separate group of spectra measured at a given excitation wavelength PCA confirmed the difference between the patterns of healthy and cancer cells, in particular in the region between 550 and 850 nm, and given that this difference seemed relatively independent on the excitation wavelength, multivariate classification was then performed to verify these findings, regardless of the specific excitation wavelengths. To this aim, the region between 550 and 850 nm was therefore considered for the calculation of two PLS-DA models, one on mean centered variables and one on autoscaled variables, and considering the whole set of spectra as described in Section 2.3.2. The results of the two PLS-DA models are reported in Table 1. Furthermore, the plots of the average classification error calculated in crossvalidation versus the number of LVs, used to define the optimal model dimensionality, are also provided as supporting information in Figures S1 and S2 for the models calculated on mean centered and on autoscaled variables, respectively.

Both the classification models showed satisfactory performances. Slightly better values were obtained in calibration and in crossvalidation with the model calculated considering the autoscaled variables, while the same results were obtained for the prediction of the test set samples, where only one healthy sample measured at $\lambda_{exc} = 470$ nm was misclassified in both the models. The SENS values, indicating the ability to correctly identify the NMSC samples, were always very high, while the SPEC ones were always lower, indicating that the largest part of misclassifications were due to the incorrect attributions of healthy samples to the NMSC class.

Interestingly, both the PLS-DA models showed very similar values of the variable importance in projection (VIP) scores [24, 25], as reported in Figure 8. The VIP scores allow to estimate the importance of each variable used in a PLS model: the variables with VIP values higher than a fixed limit (usually set equal to 1) are considered significant for the model. The LVs of the two PLS-DA models are also provided as supporting information in Figures S3 and S4 for the models calculated on mean centered and on autoscaled variables, respectively. Furthermore, in Figures S5 and S6 of the supporting information file are also reported the plots of percentage of y captured variance versus the number LVs for the two models. For both the models, the VIP scores suggest that the spectral region significantly contributing to the

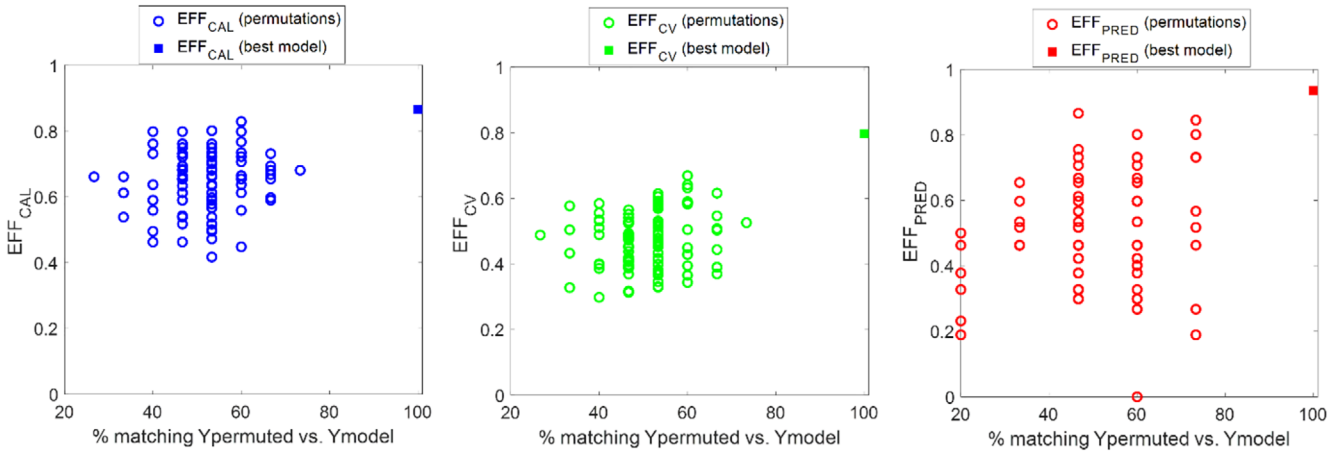

FIGURE 9 Comparison of the classification efficiency values obtained for the best PLS-DA model (full squares) with the corresponding values obtained with the permutation test (empty circles). The plot on the left reports the EFF_{CAL} values (blue); the central plot reports the EFF_{CV} values (green), and the plot on the left reports the EFF_{PRED} values (red)

TABLE 2 Results of the one-tailed *t* test performed on the EFF_{CAL}, EFF_{CV}, and EFF_{PRED} values reported in Figure 8

		Permutations		One tailed *t* test		
	Best model	**m**	**s**	t_{CRIT}*	t_{CALC}	$P(t_{CALC})$
EFF_{CAL}	0.866	0.646	0.089	1.660	2.459	7.84×10^{-3}
EFF_{CV}	0.797	0.472	0.086	1.660	3.761	1.43×10^{-4}
EFF_{PRED}	0.935	0.488	0.160	1.660	2.789	3.17×10^{-3}

*$p = 0.05$; df = 99.

discrimination between NMSC and healthy cells is between 550 and 670 nm. The two peaks, centered at about 590 and 650 nm, are very close to the peaks of lipo-pigments (580 nm) and of porphyrins (650 nm), respectively, as it was previously discussed in the comments to Figure 4B. Furthermore, the high values between 550 and 570 nm could be ascribable to the peak of FAD, which has a maximum centered at about 530 nm.

Finally, the statistical significance of the best performing classification model, that is, of the PLS-DA model calculated on the autoscaled variables, was further checked by means of a permutation test. Figure 9 shows the results of the permutation test, where the EFF values of the correct model (full squares) and of the permutations (empty circles) are reported as a function of the percentage of matching between the correct class assignation and the randomly shuffled one.

To evaluate whether the EFF values obtained for the correct model (i.e., the best PLS-DA model) were statistically significant, they were compared with the distribution of the corresponding EFF values from permutations, using a one-tailed *t* test.

Table 2 reports the EFF values obtained with the best PLS-DA model, the mean (*m*) and standard deviation (*s*) of the EFF values obtained with the permutation test, and the corresponding results of the one-tailed *t* tests. The results confirm that the significance of the EFF values obtained with the best PLS-DA model is much lower than 0.05, that is, that the good performance of the selected classification model is not due to chance.

4 | CONCLUSION

AF excited with different wavelengths was used to discriminate between normal and NMSC (SCC) cells cultivated in vitro. AF was measured on cells both suspended in their saline solution or on cell pellets. For all excitation wavelengths a coherent and distinctive picture is obtained, where normal cells clearly show characteristic features that are associated with typical chromophores [FAD and NAD(P)H, lipo-pigments, porphyrins] that are severely attenuated and smeared out in pathological cells. This is particularly evident in the AF spectra acquired using UV excitation wavelengths. Since the overall AF intensity signal can vary significantly in different replicas of the same type of samples, and with the idea of making AF a fast and reliable method for fast diagnosis of NMSC, multivariate analysis was performed on a series of datasets obtained on different freshly prepared replicas of control and SCC cells samples. The multivariate classification models calculated using PLS-DA allowed us to distinguish between the two families of AF curves related to healthy and pathological cells, independently on overall spectral intensity and excitation wavelength. Due to the relatively limited

number of available samples, the best classification model was further tested by means of a permutation test, whose results were then verified by a one-tailed *t* test that confirmed its statistical significance ($p = 0.003$ for the prediction of the test set samples). In particular it was possible to identify between 550 and 670 nm the AF spectral region which is more meaningful to separate the two families. Indeed, this is the region where contributions from FAD, lipo-pigments and porphyrins show up. We believe that these findings, where the signal of the cells is isolated from the rest of the matrix, can give valuable contribution to the understanding of the complex AF signal originated in normal and cancerous skin tissues. This could provide a further tool toward the application of AF in fast and noninvasive diagnosis of skin cancer.

AUTHOR CONTRIBUTIONS

Federico Garbarino and Alessia Paganelli were involved in the investigation and writing. Daniel Scelfo was involved in the experimental investigation. Gabriele Paulone was involved in the multivariate analysis. Cristina Magnoni, Alessandro Ulrici, and Luca Pasquali contributed equally in the conceptualization, investigation, writing—review and editing.

ACKNOWLEDGMENTS

We acknowledge financial support of the project FAR2019—INTER—line FCRM, title "LUMINA". Open Access Funding provided by Universita degli Studi di Modena e Reggio Emilia within the CRUI-CARE Agreement.

CONFLICT OF INTEREST

The authors declare no financial or commercial conflict of interest.

DATA AVAILABILITY STATEMENT

The data that support the findings of this study are available from the corresponding author upon reasonable request.

ORCID

Luca Pasquali https://orcid.org/0000-0003-0399-7240

REFERENCES

[1] A. C. Croce, G. Bottiroli, *Eur. J. Histochem.* **2014**, *58*, 320.
[2] M. Monici, *Biotechnol. Annu. Rev.* **2005**, *11*, 227.
[3] N. Ramanujam, *Neoplasia* **2000**, *2*, 89.
[4] H. Zeng, C. MacAulay, B. Palcic, D. I. McLean, *Photochem. Photobiol.* **1995**, *61*, 639.
[5] M. Meleti, I. Giovannacci, P. Vescovi, G. Pedrazzi, P. Govoni, C. Magnoni, *Oral Dis.* **2020**, *26*, 1185.
[6] M. Panjehpour, C. E. Julius, M. N. Phan, T. Vo-Dinh, S. Overholt, *Lasers Surg. Med.* **2002**, *31*, 367.
[7] H. J. C. M. Sterenborg, M. Motamedi, R. F. Wagner, M. Duvic, S. Thomsen, S. L. Jacques, *Lasers Med. Sci.* **1994**, *9*, 191.
[8] E. A. Drakaki, C. Dessinioti, A. J. Stratigos, C. Salavastru, C. Antoniou, *J. Biomed. Opt.* **2014**, *19*, 030901. https://doi.org/10.1117/1.JBO.19.3.030901
[9] C. F. Poh, L. Zhang, D. W. Anderson, J. S. Durham, P. M. Williams, R. W. Priddy, K. W. Berean, S. Ng, O. L. Tseng, C. MacAulay, M. P. Rosin, *Clin. Cancer. Res.* **2006**, *12*, 6716.
[10] W. Franco, E. Gutierrez-Herrera, N. Kollias, A. Doukas, *Br. J. Dermatol.* **2016**, *174*, 499.
[11] H. W. Rogers, M. A. Weinstock, S. R. Feldman, B. M. Coldiron, *JAMA Dermatol* **2015**, *151*, 1081.
[12] E. Borisova, P. Pavlova, E. Pavlova, P. Troyanova, L. Avramov, *Int. J. Bioautomation* **2012**, *16*, 53.
[13] I. Giovannacci, M. Meleti, F. Garbarino, A. M. Cesinaro, E. Mataca, G. Pedrazzi, C. Reggiani, A. Paganelli, A. Truzzi, F. Elia, L. Giacomelli, C. Magnoni, *Cancers* **2021**, *13*, 3974.
[14] N. V. Chernomyrdin, A. D. Lesnichaya, E. V. Yakovlev, K. G. Kudrin, O. P. Cherkasova, E. N. Rimskaya, V. N. Kurlov, V. E. Karasik, I. V. Reshetov, V. V. Tuchin, K. I. Zaytsev, *J. Biomed. Photonics Eng.* **2019**, *5*, 010302.
[15] J. L. Jayanthi, R. J. Mallia, S. T. Shiny, K. V. Baiju, A. Mathews, R. Kumar, P. Sebastian, J. Madhavan, G. N. Aparna, N. Subhash, *Lasers Surg. Med.* **2009**, *41*, 345.
[16] N. Ramanujam, M. F. Mitchell, A. Mahadevan-Jansen, S. L. Thomsen, G. Staerkel, A. Malpica, T. Wright, N. Atkinson, R. Richards-Kortum, *Photochem. Photobiol.* **1996**, *64*, 720.
[17] I. Giovannacci, C. Magnoni, P. Vescovi, A. Painelli, E. Tarentini, M. Meleti, *Arch. Oral Biol.* **2019**, *105*, 89.
[18] B. L. Meena, A. Agarwal, C. Pantola, K. Pandey, A. Pradhan, *J. Biomed. Opt.* **2019**, *24*, 035008.
[19] A. C. Croce, G. Santamaria, U. De Simone, F. Lucchini, I. Freitas, G. Bottiroli, *Photochem. Photobiol. Sci.* **2011**, *10*, 1189.
[20] Q. He, H. Lui, D. Zloty, B. Cowan, L. Warshawski, D. I. McLean, H. Zeng, Proceedings SPIE 6534, Fifth International Conference on Photonics and Imaging in Biology and Medicine. **2007**, *653413*. https://doi.org/10.1117/12.741593
[21] H. Zeng, D. I. McLean, C. E. MacAulay, B. Palcic, H. Lui, Proceedings SPIE 3245, Lasers in Surgery: Advanced Characterization, Therapeutics, and Systems VIII. **1998**, *3245*. https://doi.org/10.1117/12.312300
[22] M. C. Skala, K. M. Riching, A. Gendron-Fitzpatrick, J. Eickhoff, K. W. Eliceiri, J. G. White, N. Ramanujam, *Proc. Natl. Acad. Sci. U. S. A.* **2007**, *104*, 19494.
[23] T. M. Johnson, A. H. Hielscher, A. A. Eick, J. R. Mourant, J. P. Freyer, D. Shen, *Appl. Opt.* **1998**, *37*, 3586.
[24] L. Pigani, A. Culetu, A. Ulrici, G. Foca, M. Vignali, R. Seeber, *Food Chem.* **2011**, *129*, 226.
[25] I. G. Chong, C. H. Jun, *Chemom. Intell. Lab. Syst.* **2005**, *78*, 103.

SUPPORTING INFORMATION

Additional supporting information can be found online in the Supporting Information section at the end of this article.

How to cite this article: F. Garbarino, D. Scelfo, G. Paulone, A. Paganelli, A. Ulrici, C. Magnoni, L. Pasquali, *J. Biophotonics* **2023**, e202200361. https://doi.org/10.1002/jbio.202200361